

Analyzing the collective emission of a single-photon source based on an ensemble of thermal Rydberg atoms

Jan A. P. Reuter,^{1,2,*} Max Mäusezahl,^{3,†} Felix Mounstilis,³ Tilman Pfau,³
Tommaso Calarco,^{1,2,4} Robert Löw,³ and Matthias M. Müller¹

¹*Peter Grünberg Institute - Quantum Control (PGI-8),*

Forschungszentrum Jülich GmbH, Wilhelm-Johnen-Straße, 52428 Jülich, Germany

²*Institute for Theoretical Physics, University of Cologne, Zùlpicher Straße 77, 50937 Cologne, Germany*

³*5th Institute of Physics and Center for Integrated Quantum Science and Technology,
University of Stuttgart, Pfaffenwaldring 57, 70569 Stuttgart, Germany*

⁴*Dipartimento di Fisica e Astronomia, Università di Bologna, 40127 Bologna, Italy*

(Dated: March 8, 2023)

An ensemble of Rydberg atoms can be excited with lasers such that it evolves into an entangled state with just one collective excitation within the Rydberg blockade radius. The decay of this state leads to the emission of a single, antibunched photon. For a hot vapor of Rubidium atoms in a micro cell we numerically study the feasibility of such a single-photon source under different experimental conditions like the atomic density distribution and the choice of electronic states addressed by the lasers. For the excitation process with three rectangular lasers pulses, we simulate the coherent dynamics of the system in a truncated Hilbert space. We investigate the radiative behavior of the moving Rydberg atoms and optimize the laser pulse sequence accordingly. We find that the collective decay of the single-excitation leads to a fast and directed photon emission. Finally, we analyze the residual double-excitations and find that they do not exhibit these collective decay properties and play only a minor deleterious role.

I. INTRODUCTION

Single-photon sources are essential components for many upcoming technologies including quantum computation [1, 2] and quantum communication [3, 4]. Most existing single-photon source platforms use single emitters that naturally emit antibunched light, e.g. NV-centers [5], quantum dots [6], single atoms [7], or single ions [8], all of them with specific advantages and disadvantages [9, 10]. Here, instead, we consider ensembles of Rydberg atoms and leverage the Rydberg blockade effect [11] to generate an entangled many-body state with only a single excitation based on the van-der-Waals interaction [12] between the atoms. The strong Rydberg-Rydberg interaction makes Rydberg atoms interesting for several applications in the field of quantum technologies [13], e.g., for entanglement generation or phase gates [14–18], quantum simulations [19–21] or single-photon sources [22–27]. While such a single-photon source has been first realized with ultra-cold atoms [25], it has been shown, that cooling might be omitted and a single-photon source with Rydberg atoms can also operate at room temperature [24, 27]. This, however, implies driving the atoms off-resonantly due to their individual Doppler shift, a finite time of flight, and movement-induced decoherence. Part of these challenges could be mitigated by an optimal pulse sequence to render the excitation process robust against this motional noise [24, 28].

In this paper we build on the work of Refs. [24, 27, 29]

and further investigate the emission behavior of single-photon sources based on room-temperature Rydberg-atom ensembles. We also investigate the influence of the excitation pulses on the phase information encoded in the entangled excited state which influences the directionality of the photon emission. Furthermore, we will also discuss the behavior of double-excitations and the emission of two photons. This has already been done by [26], albeit with a different approach and in a slightly different context. We start by describing the setup and our model of the system in section II. In section III we discuss our numerical approach to simulate the quantum many-body dynamics of the atomic ensemble. Finally, in section IV we present and discuss the results of the simulations both for the emission of a single-photon as well as a two-photon emission.

II. SYSTEM SETUP AND MODEL

We consider N neutral ^{85}Rb atoms in a microscopic vapor cell at room temperature as shown in Fig. 1a. In one direction the atoms are confined by cell walls that have a distance of $1\text{ }\mu\text{m}$. Three lasers couple the ground state $|g\rangle = |5S_{1/2}\rangle$ to the Rydberg state $|r\rangle = |40S_{1/2}\rangle$ via an intermediate state $|i\rangle$, and finally to the excited state $|e\rangle$ (Fig. 1b). This procedure is also known as four-wave mixing [30, 31] where $\mathbf{k}_0 = \mathbf{k}_1 + \mathbf{k}_2 - \mathbf{k}_3$ is the mixed wave vector of the three incoming lasers. For the transition from the ground to the Rydberg state we choose the first laser to be red-detuned by 100 GHz and the second laser blue-detuned also by 100 GHz, so that the two-photon transition is resonant again. This procedure minimizes the amount of population in the inter-

* ja.reuter@fz-juelich.de

† mmausezahl@pi5.physik.uni-stuttgart.de

mediate state and makes the two-photon transition more robust. For the intermediate and excited states we consider two options: either $|i\rangle = |5P_{1/2}\rangle$, $|e\rangle = |5P_{3/2}\rangle$ or $|i\rangle = |6P_{1/2}\rangle$, $|e\rangle = |6P_{3/2}\rangle$. The resonant transition frequencies have been taken from experimental data [32, 33] for the $|g\rangle \leftrightarrow |i\rangle, |e\rangle$ transitions and calculated using the ARC [34] for $|i\rangle, |e\rangle \leftrightarrow |r\rangle$.

The atoms are initially prepared in the ground state $|G\rangle := |g_1 \dots g_N\rangle$ with the goal to exploit the Rydberg blockade to create an entangled state which contains exactly a single excitation and stores the directional information of the incoming photons in the relative phases. This entangled state is the W-state $|W(t_W)\rangle = \sum_n w_n e^{i\mathbf{k}_0 \mathbf{R}_n(t_W)} |e_n\rangle$, where $\mathbf{R}_n(t)$ is the position of atom n at time t , t_W depends on the laser pulses as will become clear in section IV, and the state $|e_n\rangle := |g_1 \dots e_n \dots g_N\rangle$ denotes a single excitation of atom n in state $|e\rangle$ with all other atoms in the ground state $|g\rangle$, and the coefficients w_n depend on the distribution of the atoms and on the laser pulses. When this W-state, which is similar to a discrete Fourier transformation of the mixed photon wave \mathbf{k}_0 , decays, a single-photon is emitted with preferred direction $\mathbf{k}_e \approx \mathbf{k}_0$. For the laser geometry, we decide to set the second and third laser anti-parallel to the first one. This minimizes the detuning of the lasers from the Doppler shift and the dephasing during the decay process [24, 29].

The working principle of the single-photon source can

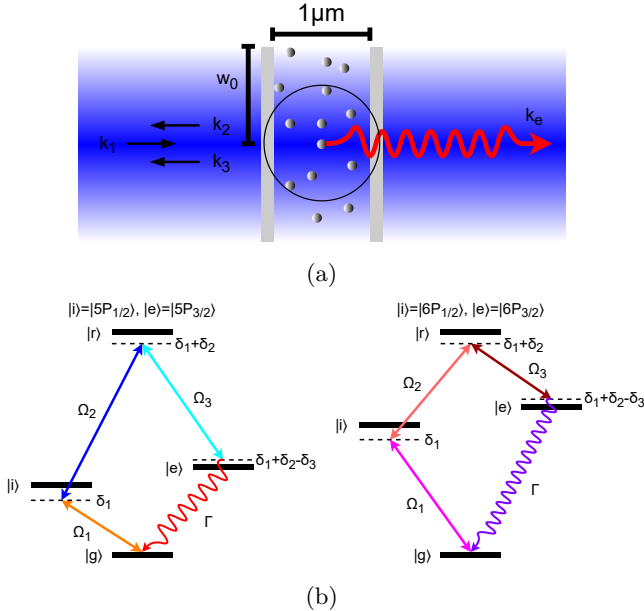


FIG. 1: Setup of the system. In (a) one can see ^{85}Rb atoms in a vapor cell which get excited by three anti-parallel lasers. The cell length as well as the laser beam waist w_0 has the size of the Rydberg blockade radius. Instead, (b) shows the two possible 4-level scheme depending on the choice of the electronic states.

be divided into two temporally subsequent steps: the excitation process from the atomic ground state $|g\rangle$ to the excited state $|e\rangle$ via photon absorption from the three lasers and the decay process back to the ground state via photon emission. This separation is valid as long as the life time τ of the excited state is much longer than the pulse duration t_0 . This is given in our case, since the two possible candidates for the excited state have a life time of $\tau_{5P} = 26.2 \text{ ns}$ [32] and $\tau_{6P} = 120.7 \text{ ns}$ [35], while we consider pulse durations around $t_0 \approx 1.5 \text{ ns}$. We will thus model the two processes separately and connect them by using the final state of the excitation process as initial state of the decay process.

A. The excitation process

The many-body Hamiltonian in the lab frame $\hat{H}(t)$ contains the transition energies \hat{H}_0 , the interaction $\hat{H}_{\text{trans}}(t) = \sum_{n,j} e\mathbf{r}_n \mathcal{E}_{j,n}(t)$ between the single valence electron with dipole moment $e\mathbf{r}_n$ of atom n with a laser field j , and the atom-atom interaction $\hat{H}_{\text{int}}(t)$. For the excitation process we describe the system in a semi-classical way, which means that we define the electric field as a classical oscillating wave $\mathcal{E}_{j,n}(t) = \mathcal{E}_j(t) \cos(\mathbf{k}_j \mathbf{R}_n(t) - \omega_j t) \epsilon_j$ with linear polarization vector ϵ_j , while we treat the electronic states as a quantum system. To simplify the calculation, we transfer the system from the lab frame to the rotating frame by a unitary transformation $|\psi(t)\rangle = \hat{T}(t)|\tilde{\psi}(t)\rangle$. We choose $\hat{T}(t)$ such that the drift part of the transformed Hamiltonian $\hat{\hat{H}}(t) = \hat{\hat{H}}_0 + \hat{\hat{H}}_{\text{trans}}(t) + \hat{\hat{H}}_{\text{int}}(t)$ takes on the form

$$\begin{aligned} \hat{\hat{H}}_0 = & -\hbar \sum_n \delta_{1,n} |i_n\rangle \langle i_n| + (\delta_{1,n} + \delta_{2,n}) |r_n\rangle \langle r_n| \\ & + (\delta_{1,n} + \delta_{2,n} - \delta_{3,n}) |e_n\rangle \langle e_n|. \end{aligned} \quad (1)$$

One can check that the choice $\hat{T}(t) = \exp(-\frac{it}{\hbar}(\hat{H}_0 - \hat{\hat{H}}_0))$ fulfills this requirement. We then apply the Rotating Wave Approximation (RWA), which neglects the fast oscillating terms from the electric field on time scales of femtoseconds and only keeps oscillations in the range of pico- up to nanoseconds. It is important to notice that one needs to transform the system back to the lab frame after the simulation to get the actual particle-dependent phases of the quantum state. The drift Hamiltonian in the rotating frame $\hat{\hat{H}}_0$ contains the detunings $\delta_{j,n} = \omega_j - \mathbf{k}_j \mathbf{v}_n$ of the different laser frequencies with respect to the resonant transitions frequencies, where we also take the Doppler shift of each particle into account. The single-atom off-diagonal elements

$$\begin{aligned} \hat{\hat{H}}_{\text{trans}}(t) = & \frac{\hbar}{2} \sum_n \Omega_{1,n}(t) |i_n\rangle \langle g_n| + \Omega_{2,n}(t) |r_n\rangle \langle i_n| \\ & + \Omega_{3,n}(t) |r_n\rangle \langle e_n| + h.c. \end{aligned} \quad (2)$$

given by the individual Rabi frequencies $\Omega_{j,n}(t) = \Omega_j(t) \exp\left(i\mathbf{k}_j \mathbf{R}_{0,n} - \frac{|\mathbf{R}_{n,j}^\perp(t)|^2}{w_{0,j}^2}\right)$ are determined by the

laser intensity, the starting position of each atom, as well as the Gaussian laser profile with beam waist $w_{0,j}$, orthogonal to its direction of propagation. Finally, the interaction energy, which doesn't change under the transformation, between two Rydberg atoms n, m is given by

$$\hat{H}_{\text{int}}(t) = \sum_{n < m} \frac{C_6}{d_{n,m}^6(t)} |r_n r_m\rangle \langle r_n r_m| \quad (3)$$

including the distance between the two atoms $d_{n,m}(t)$ and coefficients $C_6 = h \cdot 642.1 \text{ MHz } \mu\text{m}^{-6}$ [36].

B. The decay process

We start again with the Hamiltonian in the lab frame $\hat{H}_d(t) = \hat{H}_{d,0} + \hat{H}_{d,\text{trans}}(t)$, where $\hat{H}_{d,0}$ contains the transition energies and $\hat{H}_{d,\text{trans}}(t)$ is the interaction between the atoms and the electromagnetic field. Since we focus on the decay of the excited state we treat the atoms as two-level systems ($|g\rangle$ and $|e\rangle$) and neglect any atom-atom interaction. To describe the decay process of the excited atoms and the photon emission we have to quantize the electromagnetic field $\mathcal{E}_n(t) = \sum_{\mathbf{k},\mu} \mathcal{E}_k \left(a_{\mathbf{k},\mu} e^{i\mathbf{k}_j \mathbf{R}_n(t)} + a_{\mathbf{k},\mu}^\dagger e^{-i\mathbf{k}_j \mathbf{R}_n(t)} \right) \epsilon_{\mathbf{k},\mu}$ with polarization $\epsilon_{\mathbf{k},\mu}$ ($\mu \in \{1,2\}$) and annihilation operator $a_{\mathbf{k},\mu}$. Consequently, the transition elements are $\hat{H}_{d,0} = \hbar\omega_e \sum_n |e_n\rangle \langle e_n| + \sum_{\mathbf{k},\mu} \hbar\omega_{\mathbf{k},\mu} a_{\mathbf{k},\mu} a_{\mathbf{k},\mu}^\dagger$. After transforming the system into the rotating frame via $\hat{T}_d(t) = \exp(-\frac{it}{\hbar} \hat{H}_{d,0})$ and applying the RWA the Hamiltonian is

$$\hat{H}_d(t) = \hbar \sum_{n,\mathbf{k},\mu} g_{\mathbf{k},\mu} \sigma_n^\dagger a_{\mathbf{k},\mu} e^{i(\mathbf{k}\mathbf{R}_n(t) - (\omega_k - \omega_e)t)} + h.c. \quad (4)$$

with the coupling constant $g_{\mathbf{k},\mu}$ between the atoms and the electromagnetic field and the lowering operator $\sigma_n = |g_n\rangle \langle e_n|$.

1. Single-excitation and single-photon emission

We first focus on the collective decay of the singly-excited states $|e_n\rangle$ to the many-body ground state $|G\rangle$ and the emission of a single-photon $|1_{\mathbf{k},\mu}\rangle$. We thus consider a general state $|\psi_e(t)\rangle = \sum_n \alpha_n(t) |e_n\rangle |0\rangle + \sum_{\mathbf{k},\mu} \beta_{\mathbf{k},\mu}(t) |G\rangle |1_{\mathbf{k},\mu}\rangle$ with one shared excitation between the atoms and the single-photon modes, where the $\alpha_n(t)$ are the coefficients for the atomic excitation and the $\beta_{\mathbf{k},\mu}(t)$ for the photon modes, respectively. At $t = t_0$, right after the laser pulses, we consider the photon mode not to be occupied, i.e., $\beta_{\mathbf{k},\mu}(t_0) = 0$. The Schrödinger equation then leads to two coupled differential equations

$$i\dot{\alpha}_n(t) = \sum_{\mathbf{k},\mu} g_{\mathbf{k},\mu} \beta_{\mathbf{k},\mu}(t) e^{i(\mathbf{k}\mathbf{R}_n(t) - (\omega_k - \omega_e)t)}, \quad (5)$$

$$i\dot{\beta}_{\mathbf{k},\mu}(t) = \sum_m g_{\mathbf{k},\mu}^* \alpha_m(t) e^{-i(\mathbf{k}\mathbf{R}_m(t) - (\omega_k - \omega_e)t)}. \quad (6)$$

We follow the calculations of [23, 24] by integrating Eq. (6) in time and insert it into (5). We then apply the Wigner-Weisskopf approximation [37, 38] which assumes only small deviations of ω_k to be present around ω_e (i.e., the photon line width is narrow compared to its central frequency). Then, using the relation $\int_0^\infty e^{-i(\omega_k - \omega_e)(t-t')} dk \approx \frac{2\pi}{c} \delta(t-t')$ leads to a finite number of coupled differential equations for the coefficients of the atomic excitation with the single-atom decay rate $\Gamma = \frac{1}{\tau}$

$$\dot{\alpha}_n(t) \approx -\frac{\Gamma}{2} \sum_m \alpha_m(t) \text{sinc}(k_e d_{n,m}(t)). \quad (7)$$

We are now interested in the population of the photon modes which have a momentum \mathbf{k} similar to \mathbf{k}_0 . The standard approach is to insert the solutions of $\alpha_n(t)$ into Eq. (6) and sum over a discrete number of $\beta_{\mathbf{k},\mu}(t)$ in the 3D momentum space up to a certain angle [23, 24]. Another approach which we want to introduce, is multiplying the time-integrated Eq. (6) with its complex conjugate. We then integrate over the whole momentum space and use the Wigner-Weisskopf approximation again to eliminate one time integral. Furthermore, we define the angle θ between \mathbf{k} and \mathbf{k}_0 and ϕ between \mathbf{k}^\perp and $\mathbf{d}_{n,m}^\perp(t)$, both orthogonal to \mathbf{k}_0 . This results in $\sum_{\mathbf{k},\mu} |\beta_{\mathbf{k},\mu}(t)|^2 \approx \int_0^\pi p(\theta, t) d\theta$ with the population density function $p(\theta, t)$ given by

$$p(\theta, t) = \frac{\Gamma}{2} \sin(\theta) \int_{t_0}^t \sum_{n,m} \alpha_n(t') \alpha_m^*(t') e^{-ik_e d_{n,m}^\parallel(t') \cos(\theta)} J_0(k_e d_{n,m}^\perp(t') \sin(\theta)) dt', \quad (8)$$

where $J_0(\varphi) = \frac{1}{2\pi} \int_0^{2\pi} e^{-i\varphi \cos(\phi)} d\phi$ is the Bessel function

of first kind. We can then split this function into two

parts: the geometrical factor $\sin(\theta)$, which is the radius of an infinitesimal slice of a unit sphere around the ensemble, and the sum over coupled singly-excited coefficients, which contains the information on the atoms and on the absorbed photon. The advantage is that we now only have to discretize in the angle θ to calculate the photon emission numerically. Furthermore, the total probability of emitted photon and remaining excitation is constant $\int_0^\pi p(\theta, t) d\theta + \sum_n |\alpha_n(t)|^2 = \sum_n |\alpha_n(t_0)|^2$ and as a consequence, the collective decay rate can be conveniently calculated from the coefficients for the atomic excitation: $\frac{\partial}{\partial t} \int_0^\pi p(\theta, t) d\theta = -\frac{\partial}{\partial t} \sum_n |\alpha_n(t)|^2$.

2. Double-excitation and two-photon emission

In more detail, after the excitation process, the population is distributed not only over a singly-excited state and some residual ground state population as considered in the previous subsection. The main additional contribution is the undesired population of doubly-excited states $|e_n, e_m\rangle$ (i.e., all atoms in the ground state except for atoms m and n), which can lead to the emission of two photons and thus are potentially detrimental for the utilization of a single-photon source. Therefore, we want to investigate the decay of such doubly-excited states and the emission of the two photons. We consider the state $|\psi_{ee}(t)\rangle = \sum_{n < m} \alpha_{n,m}(t) |e_n, e_m\rangle |0\rangle + \sum_{n, \mathbf{k}, \mu} \beta_{n, \mathbf{k}, \mu}(t) |e_n\rangle |1_{\mathbf{k}, \mu}\rangle + \sum_{\mathbf{k}, \mu, \mathbf{q}, \eta} \gamma_{\mathbf{k}, \mu, \mathbf{q}, \eta}(t) |G\rangle |1_{\mathbf{k}, \mu}, 1_{\mathbf{q}, \eta}\rangle$, where the $\alpha_{n,m}(t)$ are the coefficients for the double-excitations of the atom, $\beta_{n, \mathbf{k}, \mu}(t)$ for the states with one atomic and one photonic excitation, and $\gamma_{\mathbf{k}, \mu, \mathbf{q}, \eta}(t)$ for the combinations of two photons with all the atoms in the ground state. Here, we neglect the fact that photons are indistinguishable, but distinguish between first $|1_{\mathbf{k}, \mu}\rangle$ (with wave vector \mathbf{k} and polarization μ) and second $|1_{\mathbf{q}, \eta}\rangle$ photon (with wave vector \mathbf{q} and polarization η), following Ref. [37]. The Schrödinger equation then leads to three coupled differential equations

$$i\dot{\alpha}_{n,m}(t) = \sum_{\mathbf{k}, \mu} g_{\mathbf{k}, \mu} \beta_{n, \mathbf{k}, \mu}(t) e^{i(\mathbf{k}\mathbf{R}_m(t) - (\omega_k - \omega_e)t)} \quad (9)$$

$$+ \sum_{\mathbf{k}, \mu} g_{\mathbf{k}, \mu} \beta_{m, \mathbf{k}, \mu}(t) e^{i(\mathbf{k}\mathbf{R}_n(t) - (\omega_k - \omega_e)t)},$$

$$i\dot{\beta}_{n, \mathbf{k}, \mu}(t) = \sum_{l \neq n} g_{\mathbf{k}, \mu}^* \alpha_{n, l}(t) e^{-i(\mathbf{k}\mathbf{R}_l(t) - (\omega_k - \omega_e)t)} \quad (10)$$

$$+ \sum_{\mathbf{q}, \eta} g_{\mathbf{q}, \eta} \gamma_{\mathbf{k}, \mu, \mathbf{q}, \eta}(t) e^{i(\mathbf{q}\mathbf{R}_n(t) - (\omega_q - \omega_e)t)},$$

$$i\dot{\gamma}_{\mathbf{k}, \mu, \mathbf{q}, \eta}(t) = \sum_l g_{\mathbf{q}, \eta}^* \beta_{l, \mathbf{k}, \mu}(t) e^{-i(\mathbf{q}\mathbf{R}_l(t) - (\omega_q - \omega_e)t)} \quad (11)$$

We then make the ansatz $\beta_{n, \mathbf{k}, \mu}(t) = \beta_{n, \mathbf{k}, \mu}^\alpha(t) \cdot \beta_{n, \mathbf{k}}^\gamma(t)$ and associate with the derivative $\dot{\beta}_{n, \mathbf{k}, \mu}^\alpha(t)$ the incoming population from the double-excitations given by the first term in Eq. (10) and with $\dot{\beta}_{n, \mathbf{k}}^\gamma(t)$ the outgoing population into the two-photon state given by the second term. We can then decouple the double-excitations in a similar way as in the single-excitation case and obtain

$$\dot{\alpha}_{n,m}(t) \approx -\frac{\Gamma}{2} \sum_{l \neq n} \alpha_{n, l}(t) \text{sinc}(k_e d_{m, l}(t))$$

$$- \frac{\Gamma}{2} \sum_{l \neq m} \alpha_{m, l}(t) \text{sinc}(k_e d_{n, l}(t)). \quad (12)$$

Furthermore, we can also decouple the remaining excitation and first-photon states from the two-photon states:

$$\dot{\beta}_{n, \mathbf{k}, \mu}(t) \approx -i \sum_{l \neq n} g_{\mathbf{k}, \mu}^* \alpha_{n, l}(t) e^{-i(\mathbf{k}\mathbf{R}_l(t) - (\omega_k - \omega_e)t)}$$

$$- \frac{\Gamma}{2} \sum_l \beta_{l, \mathbf{k}, \mu}(t) \text{sinc}(k_e d_{n, l}(t)). \quad (13)$$

Also here, we can calculate a photon-population density function for the first photon and in principle, also for the second photon. Nevertheless, we will not present the formula for the second photon since, unfortunately, it is in any case not feasible to calculate it numerically (as we will do in Sec. IV for Eq. (8) and (14)) since we would have to sum over all particle pairs twice leading to an order of $\mathcal{O}(N^4)$ terms and double time-integrals over them. The density function for the first photon is given by

$$p_2(\theta, t) = \frac{\Gamma}{2} \sin(\theta) \int_{t_0}^t \sum_n \sum_{m, l \neq n} \alpha_{n, m}(t') \alpha_{n, l}^*(t') e^{-ik_e d_{m, l}^\parallel(t') \cos(\theta)} J_0(k_e d_{m, l}^\perp(t') \sin(\theta)) dt'. \quad (14)$$

However, we can approximate the emission rate of the second photon by integrating over all first photon modes, where $\beta_{n, \mathbf{k}_e}^\gamma(t)$ is the mean value of $\beta_{n, \mathbf{k}}^\gamma(t')$ over all di-

rections:

$$\sum_{\mathbf{k}, \mu, \mathbf{q}, \eta} \partial_t |\gamma_{\mathbf{k}, \mu, \mathbf{q}, \eta}(t)|^2 = \Gamma \sum_n \sum_{\substack{m \neq n \\ l \neq n}} \quad (15)$$

$$\int_{t_0}^t \alpha_{n, m}(t') \alpha_{n, l}^*(t') \frac{\partial_t |\beta_{n, \mathbf{k}_e}^\gamma(t)|^2}{|\beta_{n, \mathbf{k}_e}^\gamma(t')|^2} \text{sinc}(k_e d_{m, l}(t')) dt'.$$

III. NUMERICAL METHODS

If we want to numerically solve the equations that we have derived in the previous section, the main challenge is the quantum many-body dynamics of the excitation process. We have to efficiently sample the atoms and find a way to effectively truncate the Hilbert space for the excitation process. The solution of the decay process instead can be found with a standard differential equation solver.

A. Particle sampling and velocity distribution

Before we simulate the excitation of the atoms via the three laser pulses, we have to sample the atoms with one of two possible distributions. The first is the standard Maxwell-Boltzmann distribution at $T = 200^\circ\text{C}$, where we assume random starting positions and a Gaussian velocity distribution in each direction. The second is produced by light-induced atomic desorption (LIAD) [39, 40] where a completely off-resonant laser pulse releases atoms which are sticking at the cell walls. For the distribution in the LIAD case, these atoms are emitted orthogonally to the glass cell walls (here also parallel to the desorption laser) leading to a directional velocity distribution $P(v, \theta) = av^2 \exp(-\frac{v^2}{b^2}) \cos(\theta)$, where we choose the parameters $a = 1.1 \times 10^{-7}$ and $b = 271 \text{ m s}^{-1}$ according to reference [40]. With that, one can calculate the time-dependent average number of atoms which have not collided into the cell walls $\langle N \rangle(t) = N_0[1 - \exp(-(\frac{\Delta x}{bt})^2)]$ if we expect that all atoms start at $t = 0$ from the wall. We set the upper limit of the complete pulse duration to 2 ns and for that 97 % of all released atoms have not collided with either cell wall. Independently of the distribution we will only simulate those particles which have not collided into the cell walls during these first 2 ns. We also only take particles into account for which the time-averaged Rabi frequency is at least 10 % of the maximum value in the middle of the Gaussian profile. For that, we consider a small beam waist of $w_{0,1} = 0.5 \mu\text{m}$ for the first laser and a broad waist $w_{0,2}, w_{0,3} = 2 \mu\text{m}$ for the second and third one. This way of choosing the beam waist ensures that only particles inside of the Rydberg blockade radius are excited to the intermediate state, but each of them then is transferred from the Rydberg state to the excited state even when they fly out of the center of the beam.

Due to the Gaussian profile of the three lasers, the motion of the atoms and the distance-dependent interaction strength of the particle pairs we have $3N + N(N-1)/2$ different time-dependent variables. Instead of treating all those variables separately, we approximate them in time and group terms by their order s , e.g. $\sum_n \Omega_{1,n}(t)|i_n\rangle\langle g_n| \approx \sum_s^{\mathcal{O}} (\sum_n \Omega_{1,n}^{(s)}|i_n\rangle\langle g_n|)t^s$. For that, we fit each variable with a polynomial up to a certain order \mathcal{O} , which was $\mathcal{O}_1 = 3$ for the first laser, $\mathcal{O}_{2,3} = 2$ for second and third laser, and $\mathcal{O}_{\text{int}} = 10$ for the interaction

energy.

B. Effective description of the low excitation sector

For the excitation process we only simulate the low excitation sector, which in our case means that we take the first two excitations fully into account and add only a third effective excitation of atoms in the intermediate state, e.g. $|i_n r_m i_l\rangle, |r_n r_m i_l\rangle$. All states with $|r_n r_m r_l\rangle, |r_n r_m e_l\rangle$ and higher will be neglected since the energy shift of three Rydberg states is much higher than the Rabi frequency of the first two lasers even for longer particle distances and so these states can never be populated for all practical purposes. Note that the notation $|i_n r_m i_l\rangle$ (and similar states) means that all atoms are in the ground state apart from the atoms m, n and l that are in the state indicated by the notation.

To describe the oscillation between a state with two arbitrary excitations n, m and the $N-2$ states with an additional atom in the intermediate state we will use third order perturbation theory, where we take the deviations of the Doppler shift from the mean velocity as perturbation (see Fig. 2 for an illustration). We define $\bar{\delta}_1 = \frac{1}{N-2} \sum_{l \neq n, m} \delta_{1,l}$ and $|\langle \Omega_1 \rangle|^2 = \sum_{l \neq n, m} |\langle \Omega_{1,l} \rangle|^2$, where $\langle \Omega_{1,l} \rangle$ are the time-averaged Rabi frequencies of each atom. Now, the eigenenergies of the Hamiltonian projected to this $(N-1)$ -dimensional subspace of the Hamiltonian without perturbation are

$$E_{\pm} = \frac{-\bar{\delta}_1 \pm \sqrt{\bar{\delta}_1^2 + |\langle \Omega_1 \rangle|^2}}{2} \quad (16)$$

and $E_{1, \dots, N-3} = -\bar{\delta}_1$. We then take $\bar{\delta}_1 - \delta_{1,l}$ as the perturbation and calculate the corrected eigenenergies E'_{\pm} to get the detuning and Rabi frequencies for the oscillations between a state with two excitations n, m and a third effective one $|i_n r_m i_{\text{eff}}\rangle$, see also Fig. 2:

$$-\bar{\delta}'_1 = E'_+ + E'_- \quad (17)$$

$$|\langle \Omega'_1 \rangle| = \sqrt{(E'_+ - E'_-)^2 - (E'_+ + E'_-)^2}. \quad (18)$$

The $N-3$ states corresponding to the eigenenergies $E'_{1, \dots, N-3}$ are dark states and not further considered.

One has to mention, that we only take the time-averaged Rabi frequency for these effective oscillations for the reason of numerical simplicity. For all other transitions (involving at maximum two excitations) we still use the time-dependent Rabi frequencies. Apart from these fast back and forth oscillations, there can be slow indirect oscillations from one state already containing an atom in the intermediate state to another. These oscillations are given by the effective Rabi frequency from the adiabatic elimination [41]

$$\hat{H}_{\text{eff}}(t) = \frac{\hbar}{4} \sum_{\substack{n \\ m < l}} \frac{\Omega_{1,l}(t)\Omega_{1,m}^*(t)}{\delta_{1,n} + \delta_{2,n} + \delta_{1,m} + \delta_{1,l}} |r_n, i_l\rangle\langle r_n, i_m| + h.c. \quad (19)$$

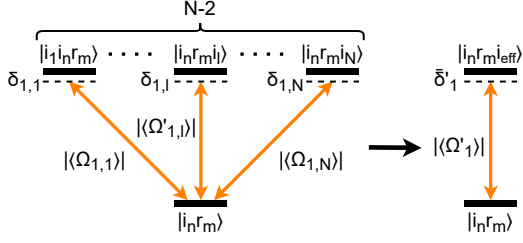


FIG. 2: Illustration of the effective description of the low-excitation sector. The oscillations from a state with two excitations, here $|i_n r_m\rangle$, to $N-2$ states with a third excitation, get combined to one oscillation to an effective state $|i_n r_m i_{\text{eff}}\rangle$.

With this effective description of the transitions one can still capture all the relevant information of the third excitation sector with a quadratic growth of the truncated Hilbert space. The solution of the time-dependent Schrödinger equation of the excitation process is then solved with Qutip [42].

IV. RESULTS

We will now present the results from the simulation and optimization of the excitation process as well as the emission properties from the decay process. Before we optimize the laser pulse sequence we first have to determine the optimal target state $W(t_W)$ by investigating the emission pattern obtained for different t_W in Sec. IV A. After that we optimize the pulse sequence and Rabi frequencies for maximal excitations and minimal phase differences of the singly-excited states in Sec. IV B. Finally, in Sec. IV C, we will use the final states from the simulation of the excitation process as initial states for the decay process and investigate the behavior of the single- and two-photon emission.

A. Optimal target state

We consider that we prepared our system with a laser pulse sequence of duration $t_0 = 1.5$ ns which drives the population into the state $\sum_{n=1} \alpha_n(t_0) |e_n\rangle$ with coefficients $\alpha_n(t_0) = \exp(i\mathbf{k}_0 \mathbf{R}_n(t_W)) / \sqrt{N}$. We then calculate the collective decay and photon emission via Eqs. (7) and (8) for different times t_W to determine the maximal photon population after several nanoseconds of decay time. Furthermore, we consider that all atoms which collide into the cell walls, from that moment do not contribute to the collective decay anymore. Fig. 3a shows that the maximal photon population reaches the detector if the phase of the atoms corresponds to a position t_W forward in time with respect to $t_0 = 1.5$ ns (i.e., $t_W > t_0$) and that its value varies by about a factor of 3 in the ana-

lyzed range of t_W . Furthermore, one can see that for the $5P$ state the emission is larger compared to the $6P$ state. The two main reasons are the much shorter life time of $5P$ as well as the longer wave length that enhances the collective decay via the sinc-term in Eq. (7). Additionally, the peak emission rate occurs at a time $t = t_p + t_0$ that is roughly proportional to $t_W - t_0$ as one can see in Fig. 3b.

In conclusion, we find that we get the most favorable emission behavior for $t_W \approx 2$ ns and thus choose this value for the parameter in our target state $W(t_W)$.

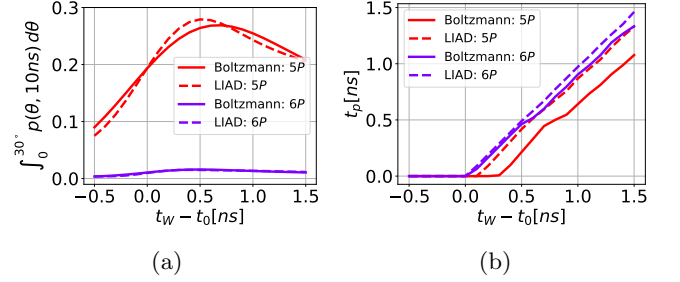


FIG. 3: Emission properties of the target state. Total photon emission after 10 ns into a forward cone up to a 30° angle to the laser direction (a) and photon emission peak position t_p (b) for different W-state phases with $N = 500$ atoms averaged over 10 samples.

B. Optimization of the pulse sequence

To optimize the pulse sequence, we first have to fix our target state $W(t_W)$. Based on the analysis of the previous section we choose $t_W = 2$ ns. Furthermore, we have to fix the weights w_n . We choose to take the time averaged Rabi frequencies $w_n = |\langle \Omega_{12,n} \rangle \langle \Omega_{3,n} \rangle| / \sqrt{\sum_n |\langle \Omega_{12,n} \rangle \langle \Omega_{3,n} \rangle|^2}$, where $\Omega_{12,n} = \Omega_{1,n} \Omega_{2,n} / (2\delta_{1,n})$ is the Rabi frequency for the two-photon transition after adiabatic elimination of the intermediate level $|i\rangle$ [41] (note that in the simulation we simulate also the intermediate level and do not actually perform the adiabatic elimination). This choice of the weights w_n reflects the influence of the laser profile and the Doppler detuning of the atoms.

We can now proceed with the optimization of the pulse sequence, where we optimize in particular the position of the three laser pulses and their amplitudes, i.e., the constant Rabi frequencies. We furthermore use the total pulse duration t_0 as an optimization parameter, and allow values out of the interval $1.25 \text{ ns} \leq t_0 \leq 1.75 \text{ ns}$. We simulate 50 different samples with 30 atoms each, where we randomly sample the positions and velocities of the atoms. We then use the mean (in the sense of an average over the 50 samples) fidelity $F_W = |\langle W(t_W) | \psi(t_0) \rangle|^2$ as Figure of Merit for a maximization with the Nelder-Mead algorithm [43] implemented in the optimization software Quantum Optimal Control Suite (QuOCS) [44].

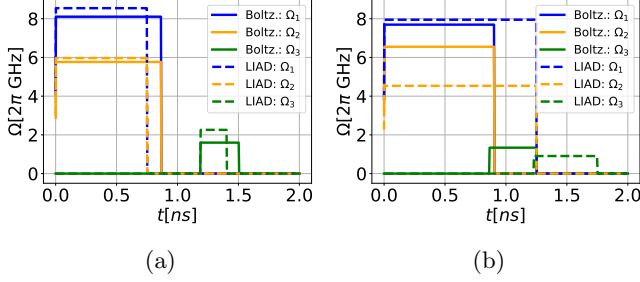


FIG. 4: The optimized pulses for the cases of the 5P (a) and 6P (b) state, obtained from the simulation of 50 samples each with $N = 30$ atoms each. The atoms were sampled once according to the Boltzmann distribution and once according to the distribution in the LIAD case and the pulses were optimized separately for all the four scenarios.

The resulting pulse shapes are shown in Fig. 4. For the 5P transitions (left panel), we can see a time gap between the end of the first two lasers, at Δt_{12} , and the start of the third one, at $t_{s,3}$. This can be explained by looking at the velocity-dependent phase of the excited state for a single atom $\phi_e(\mathbf{v}) \approx [\mathbf{k}_0 \Delta t_{12} - \mathbf{k}_3(2t_{s,3} + \Delta t_3 - \Delta t_{12})] \frac{\mathbf{v}}{2}$ (see Appendix A). Since we have an anti-parallel laser geometry, $-\mathbf{k}_3$ has the same direction as \mathbf{k}_0 . The difference between the two level schemes is that for the 5P transitions $k_3 > k_0$ and for 6P $k_3 < k_0$. Therefore, the corresponding phase time $t_\phi = \frac{\phi_e(\mathbf{v})}{\mathbf{k}_0 \cdot \mathbf{v}}$ can be noticeably greater than the pulse duration $t_0 = t_{s,3} + \Delta t_3$ if $t_{s,3} > \Delta t_{12}$. While this calculation is for a single atom, the same consideration holds also for the many-body state where we can numerically calculate how the pulse duration and timing contribute to obtaining the phases that correspond to the parameter t_W of the target state. The fidelities and the phase times are given in Tab. I.

TABLE I: The fidelity F_W , the phase time and its difference to the pulse duration. The phase time for the 5P cases are close to the desired 2 ns, while for the 6P cases its even smaller than the pulse duration.

	Boltz. 5P	LIAD 5P	Boltz. 6P	LIAD 6P
F_W	0.796	0.713	0.064	0.085
t_ϕ [ns]	1.972	1.928	0.704	0.984
$t_\phi - t_0$ [ns]	0.468	0.524	-0.548	-0.766

C. Atom decay and photon emission

To calculate the decay of the atomic excitation and the photon emission we first take the optimized pulses from the previous section and simulate the excitation process of 100 samples with each $N = 100$ atoms. Since in a real experiment the number of atoms is at least a factor of 10

higher and coefficients $\alpha_n(t_0)$ of the singly-excited states are nearly independent from each other (but depend on the velocity and initial position of each individual atom), one can group 10 samples together and only needs to divide the coefficients $\alpha_n(t_0)$ by a factor $\sqrt{10}$ to obtain a realistic estimate for the single-excitation contribution of a 1000-atoms ensemble. We can take this state as initial state to calculate the decay process, where we thus consider 10 different samples with 1000 atoms each. For the doubly-excited states we do not group the samples together because of the quadratically growing number of atom pairs $N(N-1)/2$ and the associated high computational cost; instead, we calculate the decay for all of the 100 samples separately.

As we can see in Fig. 5a there is a difference between the single-photon population density function [Eq. (8)] of the 5P and the 6P states. While for the 5P states a large amount of population is emitted with a small polar angle to \mathbf{k}_0 , it is not the case for the 6P states. The emitted population up to an angle of $\theta = 30^\circ$ is for 5P: 0.1422 in the case of Boltzmann and 0.1941 in case of LIAD, while for 6P: 0.0025 in the case of Boltzmann and 0.0021 in the case of LIAD. This difference in the photon direction seems to be correlated to the occurrence of a super-radiant emission burst during the first few nanoseconds, Fig. 5b, where the collective decay rate

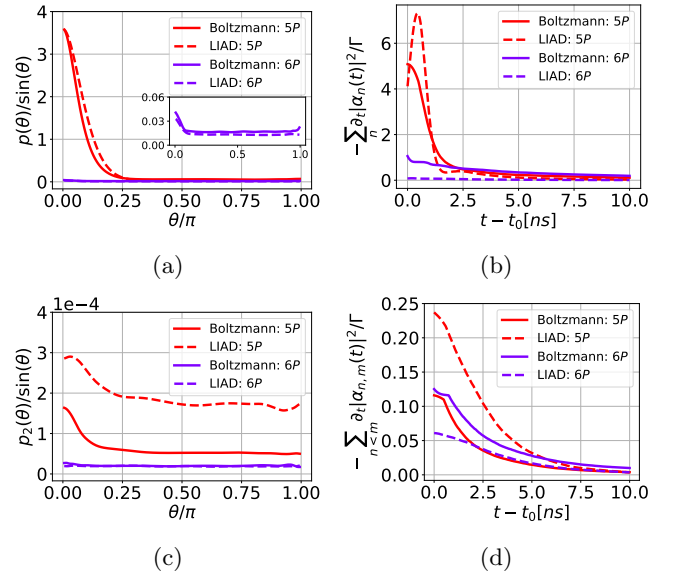


FIG. 5: Single-photon emission. (a) shows the photon-population density function from the decay of a single excitation after 10 ns where we excluded the geometrical factor $\sin(\theta)$. The inset shows the data for the 6P state on a different scale. The associated emission rate in units of the corresponding single-atom decay rate is shown in (b). (c) shows the photon population density function for the first photon coming out of the double-excitation, while the corresponding emission rate is shown in (d).

is several times larger than the single-atom decay rate Γ . This is much more pronounced for $5P$ because of the higher decay rate of the $5P$ state (i.e., the decay is faster than the dephasing due to the motion of the atoms) as well as the larger wavelength. This larger wavelength leads to a broader sinc-term in the coupling between the atoms (see Eq. (7)) which increases the collective decay rate. Additionally, it is also important that the phase corresponds to a time larger than the pulse duration in the $5P$ case, while it is smaller in the $6P$ case. One has to say that we neglected possible photon emissions induced through atom-atom and atom-wall collisions.

In Fig. 5c we show the photon population density function $p_2(\theta)$, Eq. (14), for the first photon from the decay of the double-excitation. Compared to the one for a single-photon, it is very close to an isotropic radiation source independent from the choice of the states. This seems not surprising, since the interaction energy results in an additional phase, which does not depend on the position and velocity of each atom on their own. With that, most of the stored information of the absorbed photons is lost through this interaction-dependent phase. One can also see that the photon emission rate is similar to an exponential function which one would get without any collective effects, Fig. 5d.

The emission rate of the second photon is shown in Fig. 6. It is very similar to what one would expect for two separately excited atoms both with an independent decay: one would get an emission rate proportional to $\Gamma(1 - \exp(-\Gamma t)) \exp(-\Gamma t)$. One reason that the emission peak obtained from the simulation occurs slightly earlier than $\ln(2)/\Gamma$, is (apart from a slightly collective behavior) the fact that we set the condition that an atom can only contribute to the collective decay before it collides with the wall.

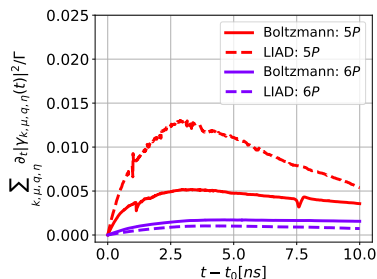


FIG. 6: Emission rate of the second photon in units of the corresponding single-atom decay rate. The second photon is emitted at a much smaller rate and with a peak at larger t compared to the single-photon. Three samples of the distribution in the LIAD case showed for the $5P$ states some numerical artefacts which we took out.

In summary, the decay of the single-excitation can show strong collective effects via in the photon direction and emission rate, while the decay of the double-excitation doesn't show these collective properties.

V. CONCLUSION

We have studied numerically the full dynamics of an on-demand single-photon source based on a room-temperature ensemble of Rydberg atoms in a micro cell. We have divided the process into the excitation and decay processes which allowed us to apply appropriate approximations for the two regimes. We have analyzed the influence of the laser pulses on the phase information of the absorbed photons and as a consequence on the directionality of the emitted photon and we have optimized the pulses accordingly. At the same time we have found that the choice of position and velocity distribution of the atoms had only a marginal effect on the photon emission.

We have investigated two different electronic level schemes, involving $5P$ and $6P$ states. Overall, we have found a considerable advantage for the $5P$ states. The main reason is a shorter lifetime or higher single-atom decay rate Γ . Furthermore, for $5P$ it is easier to encode a phase time t_ϕ greater than the pulse duration t_0 into the collective excited state (see Tab. I) which extends the time interval of directed emission, and the emitted photons have a longer wavelength $2\pi/k_e$ which increases the collective decay via the sinc-coupling of atoms. We have extended existing treatments of the decay process for a Rydberg-based single-photon source to include more rigorously the effect of motion of the atoms and described also the emission of a second photon from a residual double-excitation. For all investigated configurations we have found that the double-excitation carries only negligible phase information and leads to an almost isotropic emission pattern. Together with the already low population of the double-excitation sector after the laser pulses, this undirected emission of the second photon further improves the quality of the single-photon source. We believe that this theoretical work can help us in a planned experiment, especially towards increasing the single-photon efficiency and distinguishing single-photon emission from multi-photon emission. One could reach more realistic results by combining the simulation of the excitation process with the atomic decay. Furthermore, it might be advantageous to use optimal control and complex pulse shapes to reduce the effects of the Doppler shift, the Gaussian laser profile, and time-dependent interaction energy. For that, the laser pulses need a high bandwidth phase and amplitude modulation system.

ACKNOWLEDGMENTS

We thank Matteo Rizzi, Felix Motzoi, and Niklas Tausendpfund for fruitful discussions. This work was funded by the German Federal Ministry of Education and Research through the program "Quantum technologies - from basic research to market" under the project FermiQP (13N15891) and "AIDAS - AI, Data Analytics and Scalable Simulation", which is a Joint Virtual Laboratory gathering the Forschungszentrum Jülich (FZJ)

and the French Alternative Energies and Atomic Energy Commission (CEA) This work is also supported by the Deutsche Forschungsgemeinschaft (DFG) via Grant No. LO 1657/7-1 under DFG SPP 1929 GiRyd.

Appendix A: Velocity-dependent phase

The velocity-dependent phase of the singly-excited states for several atoms, which we mentioned in section IV B, can be derived from the calculation of a single one. For that, we will now shortly recap the time evolution of a single atom with ground state $|g\rangle$ and excited state $|e\rangle$. The transition is driven by a laser with Rabi frequency Ω and detuning δ . Furthermore, we make the exception that we start in the ground state at time t_s . The Hamiltonian looks like

$$\hat{H} = -\hbar\delta|e\rangle\langle e| + \frac{\hbar}{2}(\Omega|e\rangle\langle g| + \Omega^*|g\rangle\langle e|) \quad (\text{A1})$$

The time evolution is then given by a unitary operator

$\hat{U}(\Delta t) = \exp(-\frac{i\hat{H}\Delta t}{\hbar})$ which takes a simple form by writing it in Pauli matrices. After we transform the system back into the lab frame by applying $\exp(-i\delta\Delta t|e\rangle\langle e|)$, the final state is

$$|\psi(t)\rangle = \left[\cos\left(\frac{\Omega_\delta}{2}\Delta t\right) - i\frac{\delta}{\Omega_\delta}\sin\left(\frac{\Omega_\delta}{2}\Delta t\right) \right] e^{i\frac{\delta}{2}\Delta t}|g\rangle - i\frac{\Omega}{\Omega_\delta}\sin\left(\frac{\Omega_\delta}{2}\Delta t\right) e^{-i\frac{\delta}{2}\Delta t}|e\rangle \quad (\text{A2})$$

with the effective Rabi frequency $\Omega_\delta = \sqrt{|\Omega|^2 + \delta^2}$. If we now set the detuning equal to $\delta = -\mathbf{k}\mathbf{v}$ and the phase of the Rabi frequency as $\Omega = |\Omega|\exp(i\mathbf{k}(\mathbf{R}_0 + \mathbf{v}t_s))$ we can see that the velocity dependent phase is given by

$$\phi_e(\mathbf{v}) = \mathbf{k}\mathbf{v}(t_s + \frac{\Delta t}{2}) = \frac{\mathbf{k}\mathbf{v}}{2}(2t_s + \Delta t) \quad (\text{A3})$$

This relation is also valid for multiple atoms with more than two levels.

-
- [1] J. L. O'Brien, *Science* **318**, 1567 (2007), <https://www.science.org/doi/pdf/10.1126/science.1142892>.
 - [2] P. Kok, W. J. Munro, K. Nemoto, T. C. Ralph, J. P. Dowling, and G. J. Milburn, *Rev. Mod. Phys.* **79**, 135 (2007).
 - [3] N. Gisin and R. Thew, *Nature photonics* **1**, 165 (2007).
 - [4] F. Cavaliere, E. Prati, L. Poti, I. Muhammad, and T. Catuogno, *Quantum Reports* **2**, 80 (2020).
 - [5] N. Mizuochi, T. Makino, H. Kato, D. Takeuchi, M. Ogura, H. Okushi, M. Nothaft, P. Neumann, A. Gali, F. Jelezko, *et al.*, *Nature photonics* **6**, 299 (2012).
 - [6] P. Senellart, G. Solomon, and A. White, *Nature nanotechnology* **12**, 1026 (2017).
 - [7] M. Hijkema, B. Weber, H. P. Specht, S. C. Webster, A. Kuhn, and G. Rempe, *Nature Physics* **3**, 253 (2007).
 - [8] H. Barros, A. Stute, T. Northup, C. Russo, P. Schmidt, and R. Blatt, *New Journal of Physics* **11**, 103004 (2009).
 - [9] M. D. Eisaman, J. Fan, A. Migdall, and S. V. Polyakov, *Review of Scientific Instruments* **82**, 071101 (2011), <https://doi.org/10.1063/1.3610677>.
 - [10] B. Lounis and M. Orrit, *Reports on Progress in Physics* **68**, 1129 (2005).
 - [11] R. Heidemann, U. Raitzsch, V. Bendkowsky, B. Butscher, R. Löw, L. Santos, and T. Pfau, *Phys. Rev. Lett.* **99**, 163601 (2007).
 - [12] T. Baluktsian, B. Huber, R. Löw, and T. Pfau, *Phys. Rev. Lett.* **110**, 123001 (2013).
 - [13] M. Saffman, T. G. Walker, and K. Mølmer, *Rev. Mod. Phys.* **82**, 2313 (2010).
 - [14] D. Jaksch, J. I. Cirac, P. Zoller, S. L. Rolston, R. Côté, and M. D. Lukin, *Phys. Rev. Lett.* **85**, 2208 (2000).
 - [15] A. Gaetan, Y. Miroshnychenko, T. Wilk, A. Chotia, M. Viteau, D. Comparat, P. Pillet, A. Browaeys, and P. Grangier, *Nature Physics* **5**, 115 (2009).
 - [16] L. Isenhowe, E. Urban, X. Zhang, A. Gill, T. Henage, T. A. Johnson, T. Walker, and M. Saffman, *Physical review letters* **104**, 010503 (2010).
 - [17] T. Wilk, A. Gaëtan, C. Evellin, J. Wolters, Y. Miroshnychenko, P. Grangier, and A. Browaeys, *Phys. Rev. Lett.* **104**, 010502 (2010).
 - [18] M. M. Müller, M. Murphy, S. Montangero, T. Calarco, P. Grangier, and A. Browaeys, *Phys. Rev. A* **89**, 032334 (2014).
 - [19] H. Labuhn, D. Barredo, S. Ravets, S. De Léséleuc, T. Macrì, T. Lahaye, and A. Browaeys, *Nature* **534**, 667 (2016).
 - [20] D. Barredo, V. Lienhard, S. De Léséleuc, T. Lahaye, and A. Browaeys, *Nature* **561**, 79 (2018).
 - [21] P. Scholl, M. Schuler, H. J. Williams, A. A. Eberharter, D. Barredo, K.-N. Schymik, V. Lienhard, L.-P. Henry, T. C. Lang, T. Lahaye, *et al.*, *Nature* **595**, 233 (2021).
 - [22] M. Saffman and T. G. Walker, *Phys. Rev. A* **66**, 065403 (2002).
 - [23] L. H. Pedersen and K. Mølmer, *Phys. Rev. A* **79**, 012320 (2009).
 - [24] M. M. Müller, A. Kölle, R. Löw, T. Pfau, T. Calarco, and S. Montangero, *Phys. Rev. A* **87**, 053412 (2013).
 - [25] Y. O. Dudin and A. Kuzmich, *Science* **336**, 887 (2012), <https://www.science.org/doi/pdf/10.1126/science.1217901>.
 - [26] F. Bariani and T. A. B. Kennedy, *Phys. Rev. A* **85**, 033811 (2012).
 - [27] F. Ripka, H. Kübler, R. Löw, and T. Pfau, *Science* **362**, 446 (2018), <https://www.science.org/doi/pdf/10.1126/science.aau1949>.
 - [28] M. M. Müller, R. S. Said, F. Jelezko, T. Calarco, and S. Montangero, *Reports on Progress in Physics* **85**, 076001 (2022).
 - [29] J. A. P. Reuter, *A single-photon source based on Rydberg atoms*, Master's thesis, University of Cologne (2022).
 - [30] A. Kölle, G. Eppe, H. Kübler, R. Löw, and T. Pfau,

- Phys. Rev. A **85**, 063821 (2012).
- [31] F. Ripka, Y.-H. Chen, R. Löw, and T. Pfau, Phys. Rev. A **93**, 053429 (2016).
 - [32] D. A. Steck, Rubidium D Line Data (2021), available online <http://steck.us/alkalidata> (revision 2.2.2, 9 July 2021).
 - [33] C. Glaser, F. Karlewski, J. Kluge, J. Grimm, M. Kaiser, A. Günther, H. Hattermann, M. Krutzik, and J. Fortágh, Phys. Rev. A **102**, 012804 (2020).
 - [34] N. Šibalić, J. Pritchard, C. Adams, and K. Weatherill, Computer Physics Communications **220**, 319 (2017).
 - [35] E. Gomez, S. Aubin, L. A. Orozco, and G. D. Sprouse, J. Opt. Soc. Am. B **21**, 2058 (2004).
 - [36] F. Ripka, *A single-photon source based on strongly interacting thermal Rydberg atoms* (Verlag Dr. Hut, 2019).
 - [37] M. O. Scully and M. S. Zubairy, *Quantum Optics* (Cambridge University Press, 1997).
 - [38] K. Jacobs and D. A. Steck, Contemporary Physics **47**, 279 (2006), <https://doi.org/10.1080/00107510601101934>.
 - [39] M. Meucci, E. Mariotti, P. Bicchi, C. Marinelli, and L. Moi, Europhysics Letters **25**, 639 (1994).
 - [40] F. Christaller, M. Mäusezahl, F. Mounstsilis, A. Belz, H. Kübler, H. Alaeian, C. S. Adams, R. Löw, and T. Pfau, Physical Review Letters **128**, 10.1103/physrevlett.128.173401 (2022).
 - [41] E. Brion, L. H. Pedersen, and K. Mölmer, Journal of Physics A: Mathematical and Theoretical **40**, 1033 (2007).
 - [42] J. Johansson, P. Nation, and F. Nori, Computer Physics Communications **184**, 1234 (2013).
 - [43] J. A. Nelder and R. Mead, The Computer Journal **7**, 308 (1965), <https://academic.oup.com/comjnl/article-pdf/7/4/308/1013182/7-4-308.pdf>.
 - [44] M. Rossignolo, T. Reisser, A. Marshall, P. Rembold, A. Pagano, P. J. Vetter, R. S. Said, M. M. Müller, F. Motzoi, T. Calarco, *et al.*, arXiv preprint arXiv:2212.11144 (2022).